Applied Surface Science xxx (xxxx) xxx-xxx

Contents lists available at ScienceDirect

Applied Surface Science

journal homepage: http://ees.elsevier.com

NO_2 gas sensors based on CVD tungsten diselenide monolayer

Yichuan Wu [a,b,c], Nirav Joshi [b,d,*], Shilong Zhao [c,e], Hu Long [e], Liujiang Zhou [f], Ge Ma [g], Bei Peng [a], Osvaldo N Oliveira Jr [d], Alex Zettl [e], Liwei Lin [b,c]

[a] School of Mechanical and Electrical Engineering, University of Electronic Science and Technology of China, Chengdu 611731, China
[b] Berkeley Sensor and Actuator Center, University of California at Berkeley, CA 94720, USA
[c] Tsinghua-Berkeley Shenzhen Institute, Tsinghua University, Shenzhen 518055, China
[d] São Carlos Institute of Physics, University of São Paulo, São Carlos 13560-970, Brazil
[e] Department of Physics, University of California at Berkeley, and Materials Sciences Division, Lawrence Berkeley National Laboratory, and Kavli Energy NanoScience Institute at the University of California Berkeley and the Lawrence Berkeley National Laboratory, Berkeley, CA 94720, USA
[f] Institute of Fundamental and Frontier Sciences, University of Electronic Science and Technology of China, Chengdu 610054, China
[g] Department of Intelligent Industrial Research, China Academy of Industrial Internet, Beijing 100084, China

ARTICLE INFO

Keywords
Two-dimensional layered WSe_2
Gas sensor
Chemical vapor deposition
Selectivity
Recovery speed

ABSTRACT

Two-dimensional (2D) transition metal dichalcogenides (TMDs) are promising for gas sensors owing to their large surface-to-volume ratios, but the long recovery times stemming from the slow molecular desorption have been an important limitation. In this work, we report on a sensor for nitrogen dioxide (NO_2) made with a diselenide (WSe_2) monolayer synthesized via chemical vapor deposition, which functions within a range of concentrations from 100 ppb to 5 ppm and at various temperatures, including room temperature. When operated at an optimized temperature of 250 °C, the WSe_2 sensor exhibited the fastest recovery, with the response (τ_{res}) and recovery (τ_{rec}) times of 18 s and 38 s, respectively, when exposed to 100 ppb NO_2. The sensor also features high selectivity toward NO_2 in the presence of other target gases, in addition to reversibility and long-term stability within 60 days. The overall characteristics of the WSe_2 sensor make it suitable to monitor indoor/outdoor environments, mainly if further optimization is made with sensor design based on a model for the sensing mechanism we present in this paper.

1. Introduction

Human beings and animals are continually exposed to environmental hazards due to air pollution and emission from gas explosion accidents [1–3]. The exposure to toxic gases may lead to cancer and lung and heart diseases, whose early diagnosis requires gas sensing in health monitoring systems [4,5]. Nitrogen dioxide (NO_2) is one of the most hazardous polluting gases, coming mainly from exhaustion. Overexposure to NO_2 has caused respiratory problems [6] as the NO_2 gas molecules can easily cause inflammation of inner linings of lungs and reduce their immunity to infections, which is particularly harmful to people with asthma. Sensitive and selective NO_2 gas sensors are therefore needed for monitoring indoor/outdoor environments to protect human health [7], which can, in principle, be exploited with the variety of materials employed in gas sensors. Selectivity and operation temperature are vital issues of the gas sensor, for example, Metal oxides possess high sensitivity towards toxic gases, but their operating temperature and selectivity are still limited [8]. Graphene-based sensors, on the other hand, exhibit poor performance at low concentrations and low recovery speed [9]. Some strategies, including surface functionalization, designing heterostructures, fabrication of nanocomposite, and utilization of metal oxides, have been employed to improve the selectivity of a sensor [10–12].

Possible alternatives for efficient gas sensors are the two-dimensional (2D) monolayered materials, especially transition metal dichalcogenides (TMDs) with the general formula MX_2 owing to their high surface area to volume ratios and susceptible large surfaces [13,14]. These 2D TMDs have been synthesized directly on silicon or glass substrates by chemical vapor deposition (CVD) [15–20], e.g., WS_2, MoS_2, $MoSe_2$, and WSe_2 were fabricated by CVD and atomic layer deposition (ALD) [21–23]. Recent works have proven that gas sensors made with 2D TMDs are sensitive to NO_2 gas, including at room temperature [24–27]. This has motivated us to institute a project and fabricate large-area and highly crystalline WSe_2 monolayers using the vapor phase reaction of WO_3 and Se carried by flowing gases in a tube furnace [28]. The rationale is to address the various factors that define the suitability of NO_2 gas sensors, namely sensitivity, selectivity, re-

* Corresponding author at: Berkeley Sensor and Actuator Center, University of California at Berkeley, CA 94720, USA.
E-mail address: nirav.joshi1986@gmail.com (N. Joshi)

https://doi.org/10.1016/j.apsusc.2020.147110
Received 4 May 2020; Received in revised form 22 June 2020; Accepted 28 June 2020
Available online xxx
0169-4332/

sponse and recovery rate, and stability. We show that sensors made with WSe_2 may be obtained with low detection limit, reproducibility, and reversibility in a wide range of NO_2 concentrations with the fastest recovery for operation at an optimized temperature.

2. Experimental details

2.1. Synthesis

A single zone furnace is shown in Fig. 1(a) was used for CVD growth of WSe_2, with Se Powders (60 mg, 99.5%, Sigma-Aldrich) loaded outside the furnace at the upstream. When the furnace temperature reached 850 °C, the furnace was moved towards the upstream with a distance of 4 cm, where the temperature of Se powders reached 300 °C. WO_3 powders (10 mg, 99.5%, Sigma-Aldrich) were loaded in the center of the furnace. The sapphire substrate was placed on top of the WO_3 upside down. The sapphire substrate was previously treated with plasma to obtain a hydrophilic surface and coated with perylene-3,4,9,10-tetracarboxylic acid tetra potassium salt (PTAS) as the seeding promoter. The tube was pumped to the vacuum of 0.05 Torr and flushed with Ar gas to ambient pressure for three times. The temperature was increased to 250 °C at a rate of 50 °C/min, kept for 20 min, and then increased to 850 °C and kept for 10 min. During the process, Ar/H_2, with the volume ratio of 85:15, was used as the carrier gas with a flow rate of 80 sccm at ambient pressure [29].

2.2. Gas sensing measurements

The gas sensing performance of WSe_2 monolayer films were evaluated in terms of the percentage sensing response, response, and recovery time. A pair of planar gold electrodes were deposited on top of the film by sputtering under a shadow mask with 2 mm spacing between electrodes, as shown in Fig. 1(b). The sensor film was wire-bonded into a dual in-line package (DIP) package and placed in a chamber with a volume of around 1 cm^3 for electrical characterization and sensing measurements. The gases used in this study include NO_2 (21 ppm in N_2), H_2 (5% in N_2), CO_2 (2000 ppm in N_2), NH_3 (200 ppm in N_2), CO (500 ppm in N_2), which are calibrated and supplied by Praxair, Inc. A computer-controlled gas delivery system was used to flow individual gas at a constant gas flow rate of 300 sccm to the sensor chamber. In total, 12 mass flow controllers (Bronkhurst) controlled by LabView are used to dilute the gas mixture cylinder with clean air and deliver these gases to the sensor chamber. The stream balance and purge consisted of house air that was dehumidified using a pressure swing adsorption dryer and decontaminated using an activated carbon scrubber. The flow stream temperature and sensor chamber temperature are recorded and are controlled within a few degrees of room temperature. The sensor signal was analyzed using a data acquisition system (Labview) with an open-source Java-based instrument (Zephyr) for controlling and obtaining the data [30]. The sensor measurements were conducted with a Keithley 2602 source meter by applying a bias voltage and recording the current, from which the resistance R was calculated. The concept image of monolayer WSe_2 sensing NO_2 molecules is shown in Fig. 1(c), and the gas sensor response (S) is defined as:

$$\text{Response}(\%) = \left[\frac{\Delta R}{R_a}\right] \times 100 \quad [1]$$

$\Delta R = R_a - R_g$ for oxidizing gases like nitrogen dioxide (NO_2), where R_g and R_a are the resistance of the sensor film under the exposure of test gas and fresh air, respectively. The response time (τ_{res}) is defined as the time taken to reach 90% of the full response after the exposure of the target gas. The recovery time (τ_{rec}) is defined as the time taken to return to 10% of the baseline resistance after the flow of target gas is stopped. The as-prepared CVD-grown WSe_2 monolayers were characterized by Tapping mode atomic force microscopy (AFM) (Multimode, Bruker, USA), Raman spectroscopy, and photoluminescence (PL) (LabRam ARAMIS, HORIBA, equipped with a 532 nm laser as excitation source). X-ray photoelectron spectroscopy (XPS) was performed using the Scienta Omicron spectrometer (model ESCA +) integrated with monochromatic Al Kα radiation (1486.6 eV) as the X-ray source for excitation. Optical microscopy (OM) images were taken using an Olympus DX51.

3. Results and discussion

Fig. 2(a) and (b) show the AFM image and height profile of WSe_2 on a sapphire substrate, where the thickness is 0.73 nm, consistent with data for mechanically exfoliated monolayered WSe_2 [28]. Fig. 2(c) shows the photoluminescence (PL) spectrum at room temperature taken with a micro-PL system (objective, 40X, NA 0.65) integrated with a 532 nm continuous wave (CW) laser, featuring a strong emission at ~ 760 nm assigned to the excitonic absorption. The Raman spectrum taken with excitation of a 473 nm laser shows the characteristic

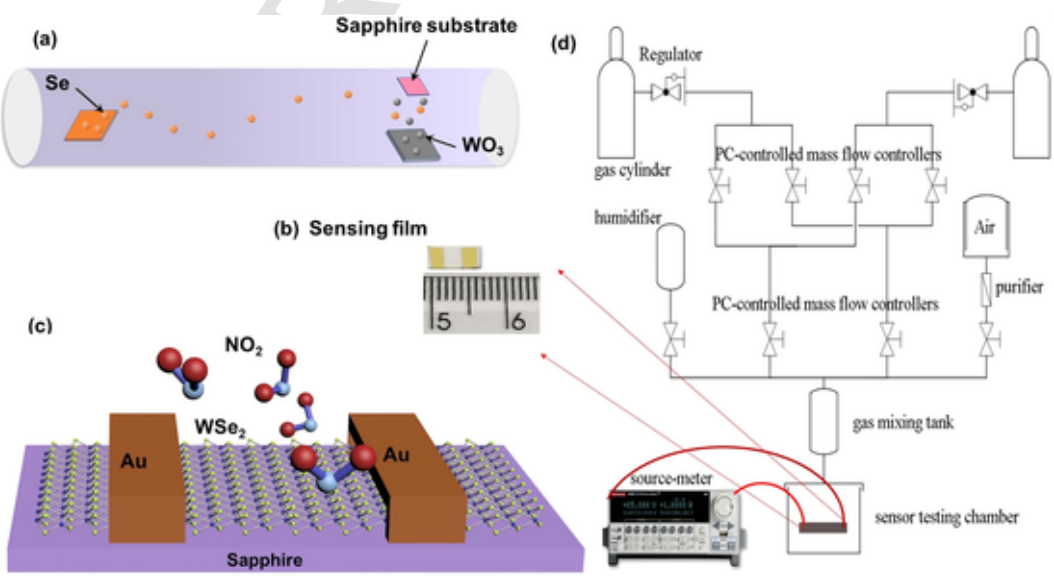

Fig. 1. (a) Schematic diagram of the fabrication process of CVD-grown WSe_2. (b) Optical image of the 7 mm × 3 mm gas sensing device. (c) A concept image of monolayer WSe_2 and the sensing behavior of NO_2 molecules (d) Experimental setup for gas sensing measurement.

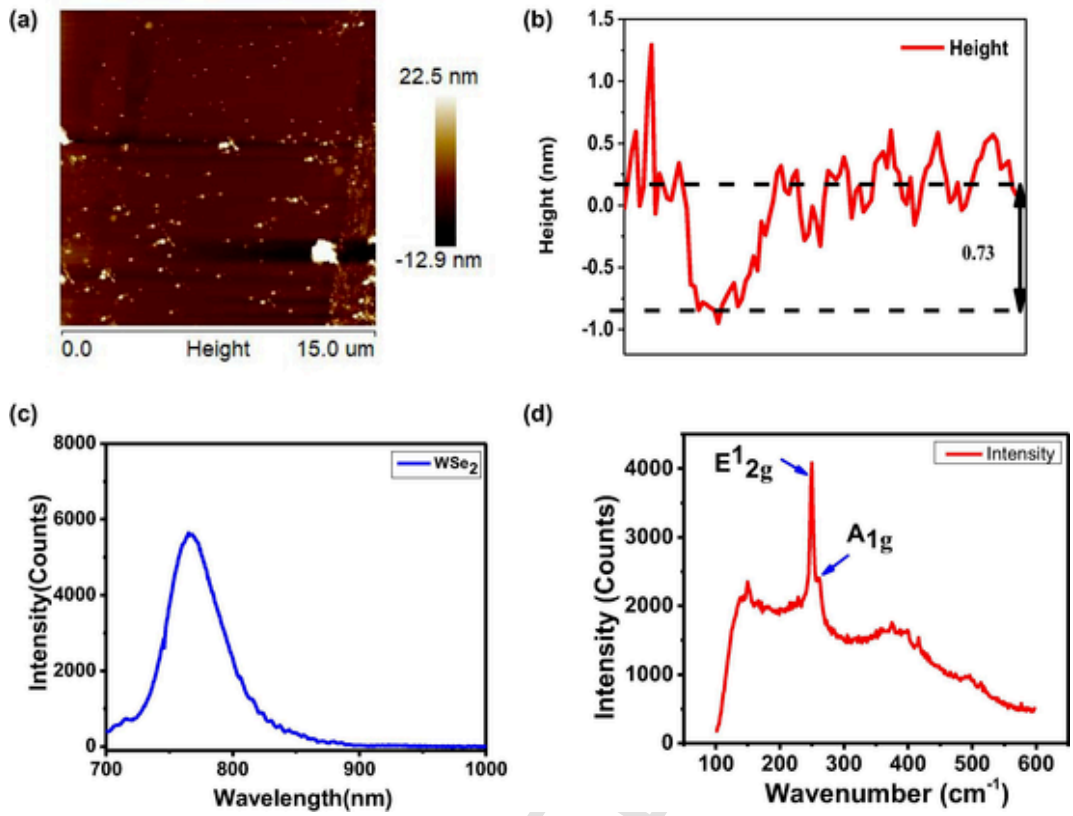

Fig. 2. Material characterizations. (a) and (b) AFM analysis images of the WSe_2 monolayer. (c) Photoluminescence spectrum for monolayer WSe_2 with a microscopic PL system (excitation wavelength 532 nm). (d) Raman spectrum for the WSe_2 monolayer obtained in a confocal Raman spectrometer excited by a 473 nm laser.

peaks for monolayer WSe_2 at 248 cm^{-1} assigned to E^1_{2g} mode and 260 cm^{-1} assigned to A_{1g} mode [31,32] in Fig. 2(d).

The XPS spectra of WSe_2 monolayer for W4f and Se 3d scans are presented in Fig. 3(a) and (b), respectively. The 3d spectra of W and Se provide information on stoichiometry and bonding. The peak energies $W4f_{7/2}$, $W4f_{5/2}$, and $W4f_{3/2}$ are located at 31.44, 33.64, and 37.19 eV, respectively, while $Se3d_{5/2}$ and $Se3d_{3/2}$ peak energies appear at 53.59 and 54.44 eV, which are typical of the semiconducting 2H phase[33–35] in WSe_2.

3.1. Gas sensing performance of WSe_2 monolayer film

The real-time resistance response of the WSe_2 film at an operating temperature of 250 °C is shown in Fig. 4(a), where the resistance decreased after exposure to NO_2 gas in a p-type semiconductor behavior[36]. Fig. 4(b) depicts linear plots for current (I) vs. voltage (V) with the WSe_2 sensor at room temperature (RT) and 250 °C, in both cases with an Ohmic contact between the WSe_2 film and the electrodes. The resistance decreases at the higher temperature, as expected for a semiconductor. Fig. 4(c) shows the sensor response for the WSe_2 film as a function of NO_2 concentrations from 0 to 5 ppm at the working temperature of 250 °C. The sensor response increases as the gas concen-

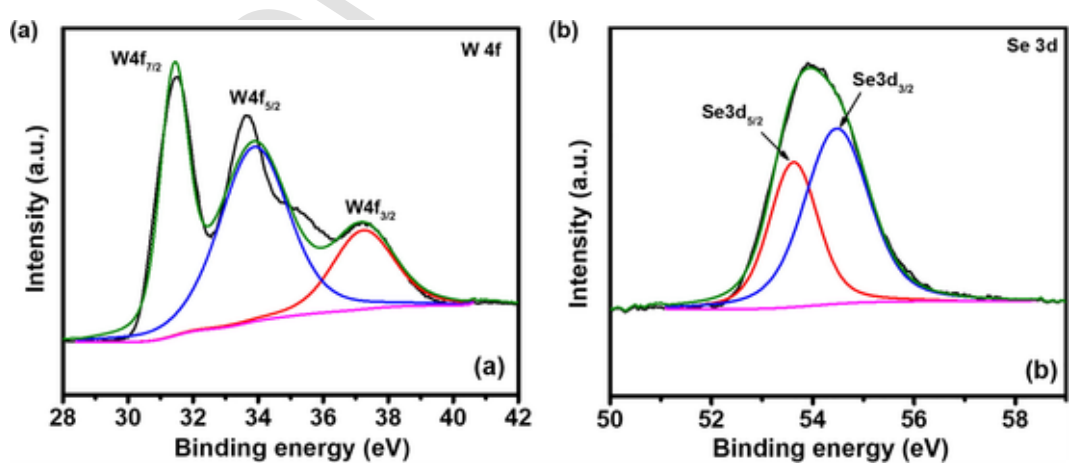

Fig. 3. The XPS spectra with fitted curves for (a) WSe_2 W4f and (b) WSe_2 Se3d scan.

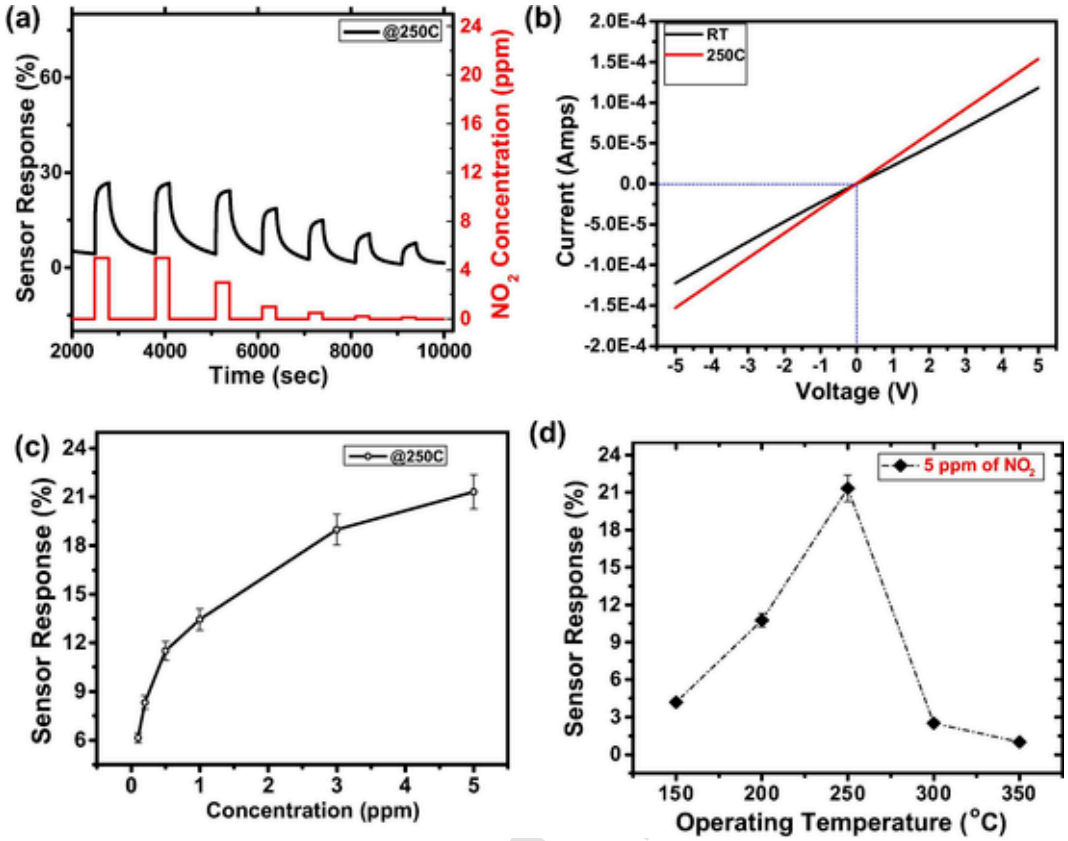

Fig. 4. (a) NO_2 gas sensing response for WSe_2 as a function of gas exposure at an operating temperature of 250 °C. (b) Linear I/V plots of the WSe_2 sensor at RT and 250 °C, respectively. (c) Sensor response versus gas concentration in the range of 0.1–5 ppm NO_2. (d) Gas sensing response of WSe_2 exposed to 5 ppm NO_2 at different operating temperatures.

tration increases, and the saturation level is almost the same as that highest concentration allowed by the current setup of the mass flux controller (MFC). For the exposure of 5 ppm NO_2, the sensor response achieves its maximum at 250 °C, according to Fig. 4(d). The sensor response achieves its maximum at 250 °C, with the appearance of a maximum being explained as follows. The reaction of NO_2 gas with chemisorbed oxygen sites increases with increasing temperatures, but above 250 °C, the desorption rate surpasses the adsorption rate. Therefore, we consider 250 °C as the optimal operating temperature where the adsorption and desorption processes reach an equilibrium. Table 1 shows a comparison of NO_2 sensing with WSe_2 and other NO_2 gas sensing materials, including MoS_2, WS_2, WSe_2, and WS_2 with graphene aerogel (GA) [24–29]. The sensor presented here is competitive with the most efficient for room temperature and displays the fastest recovery at an optimized temperature (250 °C).

For completeness, we show the gas sensing responses to NO_2 (5 and 2 ppm) at room temperature in Figure S1, as well as the reversibility and stability of the WSe_2 film sensor. Figure S2 depicts the dynamic electrical response for several NO_2 exposures (5, 5, 1, 0.1, and 5 ppm) at an operating temperature of 250 °C. After the sensor was exposed to 5 ppm NO_2 for 5 sensing cycles, it could still detect lower NO_2 concentrations, as shown in Figure S3. Since more NO_2 molecules interacted with adsorbed oxygen ions at the low concentration (0.1 ppm), a faster response time of 38 s was measured compared to that at a higher concentration (2 ppm). There was an irreversible chemical reaction, and the baseline resistance did not change. Fig. 5(a) shows enlarged response and recovery curves for the WSe_2 sensor at 5 ppm NO_2, for

Table 1
comparison of NO_2 gas sensor parameters for a WSe_2 compound with other 2D materials.

Materials	NO_2 concentration (ppm)	Recovery speed (min.)	Sensor response (%)	Reference	Operating Temp. (^{0}C)
WS_2	10	–	84.7	[27]	RT
MoS_2	100	No Recovery	~14	[37]	RT
WS_2/GA	2	5	3	[38]	180
WS_2/GA	2	Incomplete	6.5	[38]	RT
WSe_2	500	85	4140	[25]	RT
WSe_2	500	21.5	–	[25]	100
WSe_2	0.05	17.5	5.06	[39]	RT
WSe_2	2	–	~10	[39]	RT
WSe_2	0.5	–	238.35	[40]	RT
WSe_2	2	24.5	18.8	**this work**	RT
WSe_2	1	4.8	13.45	**this work**	250
WSe_2	0.1	0.63 (38 s)	6.15	**this work**	250

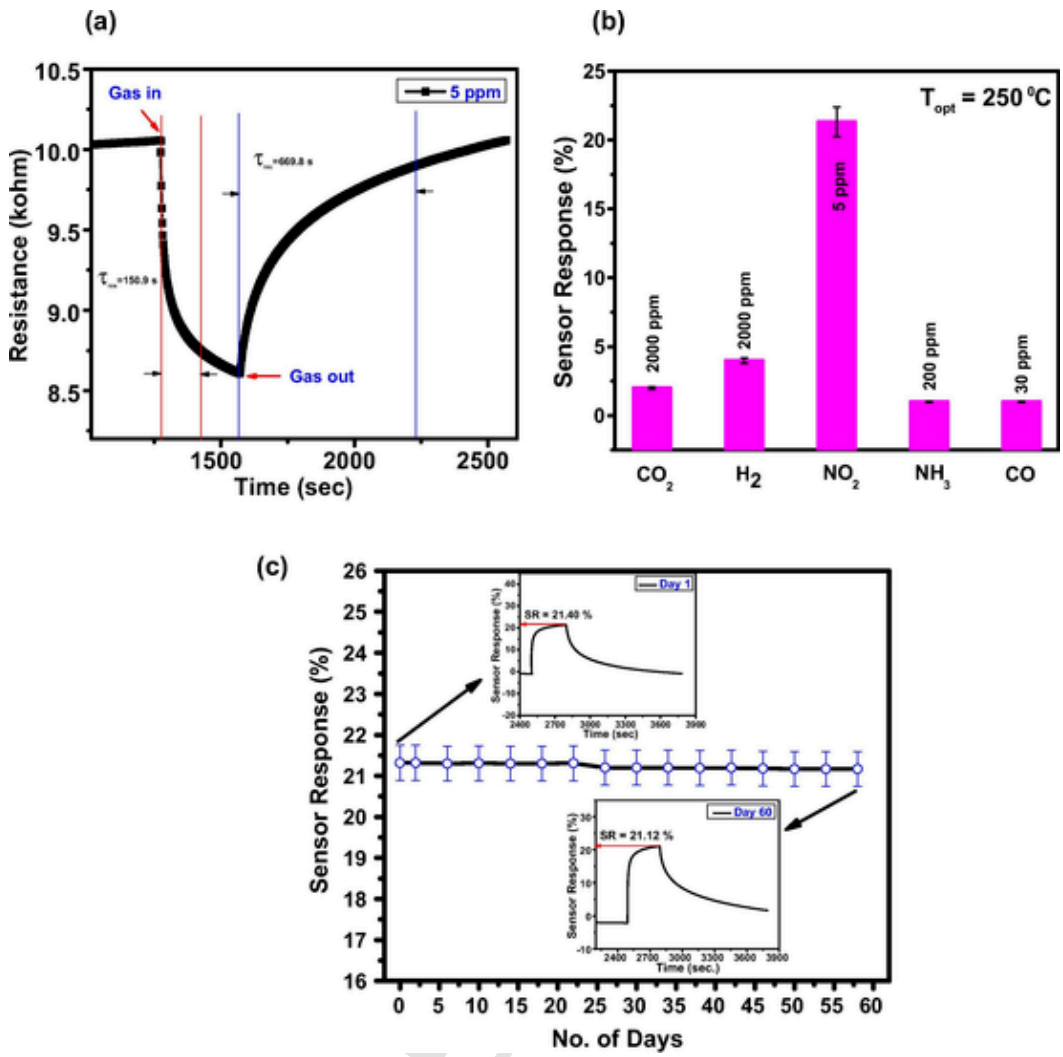

Fig. 5. (a) Typical response-recovery characteristics of WSe_2 sensor at an operating temperature of 250 °C. (b) Sensing histogram of the WSe_2 sensor exposed to common gases present in the atmosphere to show good selectivity with NO_2 (c) Long-term stability of WSe_2 monolayer to 5 ppm of NO_2 at 250 °C for 60 days.

an improvement in the recovery time. The transient responses under 5 ppm of NO_2 also reveal the stable response and recovery characteristics. The corresponding response (τ_{res}) and recovery (τ_{rec}) times were 150.9 s and 669.8 s for 5 ppm, and 18 s and 38 s for 0.1 ppm NO_2 concentration, respectively. The response and recovery time as a function of NO_2 concentrations shows in Fig. S4, it can be seen that the response time increases with increasing ozone concentration. The response time increases from 18 to 150.9 s while recovery time also increases from 38 to 669.8 sec as the concentration increases from 0.1 to 5 ppm. However, at low concentration, more NO_2 molecules easily interact with adsorbed oxygen ions providing a fast response compared to higher concentration [41,42].

Fig. 5(b) indicates the selectivity of the WSe_2 sensor toward NO_2 gas when exposed to 2000 ppm of CO_2 and H_2, 200 ppm of NH_3, and 30 ppm of CO gases and 5 ppm of NO_2 gas at 250 °C. The response to NO_2 is higher than for other oxidizing and reducing gases because of its higher adsorption energy and degree of charge transfer [25,43], as expected from density functional theory (DFT) calculations [43]. The long-term stability of WSe_2 nanosheets is confirmed in Fig. 5(c) for ten measurements for two months with 5 ppm NO_2. It can be seen that no apparent decline in the response in day one and day 60 (inset Fig. 5(c)).

Regarding the gas sensing mechanism, exposure to the oxidizing gas (NO_2) induced a decrease in resistance, which indicates a typical p-type sensing behavior [44] and an increase in resistance, which indicates n-type sensing behaviour [45,46]. There is also an unpaired electron on the nitrogen atom, which works as an electron acceptor, which allows us to propose the mechanism of Fig. 6. Electrophilic NO_2 molecules and oxygen species are spontaneously adsorbed and capture electrons from the conduction band, thus causing an increase in the concentration of holes, the majority carriers in p-type WSe_2. A hole-accumulation layer is created at the surface of WSe_2 due to chemisorption of NO_2, and the resistance decreases. The scheme depicted in Fig. 6 also explains the slow recovery of WSe_2 at room temperature. With the high adsorption energy and charge transfer, the sensor resistance starts recovering slowly because of defects on the surface of WSe_2 exposed to NO_2 molecules. Hence, the slow recovery is due to the strong adsorption of NO_2 and WSe_2 [25,47]. The scheme we present here is only pictorial since other effects from chemisorption, physisorption, defect sites, and transduction should be considered to determine the whole adsorption/desorption mechanism [48].

$$NO_{2\,(gas)} + e^- \rightarrow NO^-_{2\,(ads)}$$

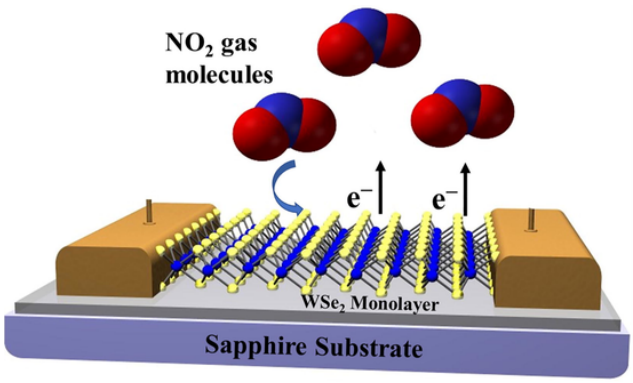

Fig. 6. Schematic picture of the sensing mechanism of WSe_2 monolayer exposed to NO_2 gas.

4. Conclusion

In this work, we reported on a high-performance WSe_2 gas sensor for NO_2, which was synthesized with the CVD process and evaluated at room temperature and high temperatures. While the sensor was competitive with other chemiresistive sensors [13,25,49,50] at room temperature, it exhibited the fastest recovery at an optimized temperature of 250 °C, also featuring fast recovery, reproducibility, and selectivity. The WSe_2 sensor works within the detection range from 0.1 to 5 ppm, thus being suitable to monitor the environment, especially when rapid detection is required, and power consumption is not a limitation. Taken together, our results confirm the expectation from the recent literature that WSe_2 is highly promising, but further studies are necessary not only to enhance the performance at room temperature but also to understand the sensing mechanisms in detail. Herein we provided a physical model that can explain qualitatively the decrease in resistance induced by the adsorption of NO_2 molecules on the WSe_2 surface, but other phenomena must be taken into account. Furthermore, new studies may be done to design WSe_2 sensors for other reducing and oxidizing gases, probably using different catalysts or tuning reaction parameters such as temperature and controlling morphology.

CRediT authorship contribution statement

Yichuan Wu: Writing - original draft, Methodology, Writing - review & editing. **Nirav Joshi:** Writing - original draft, Validation, Conceptualization, Writing - review & editing, Supervision, Investigation. **Shilong Zhao:** Methodology, Writing - original draft. **Hu Long:** Methodology, Software, Validation, Writing - review & editing. **Liujiang Zhou:** Writing - review & editing, Validation. **Ge Ma:** Writing - review & editing, Validation. **Bei Peng:** Writing - review & editing, Validation. **Osvaldo N Oliveira Jr:** Writing - review & editing, Supervision, Project administration. **Alex Zettl:** Writing - review & editing, Supervision, Project administration. **Liwei Lin:** Writing - review & editing, Supervision, Project administration.

Declaration of Competing Interest

The authors declare that they have no known competing financial interests or personal relationships that could have appeared to influence the work reported in this paper.

Acknowledgements

This work was supported by the Director, Office of Science, Office of Basic Energy Sciences, Materials Sciences and Engineering Division, of the U.S. Department of Energy under Contract No. DE-AC02-05-CH11231, within the sp2-Bonded Materials Program (KC2207), which provided for gas sensor response characterization. This work was also supported in part by the Berkeley Sensor and Actuator Center (BSAC), an Industry/University Research Cooperation Center. N.J was supported by the Sao Paulo Research Foundation (FAPESP) (grant no. 2014 / 23546-1, 2016/23474-6).

Appendix A. Supplementary data

Supplementary data to this article can be found online at https://doi.org/10.1016/j.apsusc.2020.147110.

References

[1] W Duan, B He, Emergency Response System for Pollution Accidents in Chemical Industrial Parks, China, Int. J. Environ. Res. Public Health 12 (2015) 7868–7885.
[2] D Singh, V Shukla, P K Panda, Y K Mishra, H-G Rubahn, R Ahuja, Carbon-phosphide monolayer with high carrier mobility and perceptible I-V response for superior gas sensing, New J. Chem. 44 (2020) 3777–3785.
[3] X Zhao, P K Panda, D Singh, X Yang, Y K Mishra, R Ahuja, 2D g-C3N4 monolayer for amino acids sequencing, Appl. Surf. Sci. 146609 (2020).
[4] D. Dias, J. Paulo Silva Cunha, Wearable Health Devices-Vital Sign Monitoring, Systems and Technologies, Sensors (Basel), 18(2018) 2414.
[5] N Joshi, T Hayasaka, Y Liu, H Liu, O N Oliveira, L Lin, A review on chemiresistive room temperature gas sensors based on metal oxide nanostructures, graphene and 2D transition metal dichalcogenides, Microchim. Acta 185 (2018) 213.
[6] J. Freddy Grajales, A. Baquero-Bernal, Inference of surface concentrations of nitrogen dioxide (NO2) in Colombia from tropospheric columns of the ozone measurement instrument (OMI), Atmósfera, 27(2014) 193-214.
[7] S S Shendage, V L Patil, S A Vanalakar, S P Patil, N S Harale, J L Bhosale, et al., Sensitive and selective NO2 gas sensor based on WO3 nanoplates, Sens. Actuators, B 240 (2017) 426–433.
[8] R Malik, V K Tomer, Y K Mishra, L Lin, Functional gas sensing nanomaterials: A panoramic view, Appl. Phys. Rev. 7 (2020) 021301.
[9] L Yang, N Yi, J Zhu, Z Cheng, X Yin, X Zhang, et al., Novel gas sensing platform based on a stretchable laser-induced graphene pattern with self-heating capabilities, J. Mater. Chem. A 8 (2020) 6487–6500.
[10] O Lupan, V Postica, M Mecklenburg, K Schulte, Y K Mishra, B Fiedler, et al., Low powered, tunable and ultra-light aerographite sensor for climate relevant gas monitoring, J. Mater. Chem. A 4 (2016) 16723–16730.
[11] E Martinelli, D Polese, A Catini, A D'Amico, C Di Natale, Self-adapted temperature modulation in metal-oxide semiconductor gas sensors, Sens. Actuators, B 161 (2012) 534–541.
[12] I Montoliu, R Tauler, M Padilla, A Pardo, S Marco, Multivariate curve resolution applied to temperature-modulated metal oxide gas sensors, Sens. Actuators, B 145 (2010) 464–473.
[13] Y Hong, W-M Kang, I-T Cho, J Shin, M Wu, J-H Lee, Gas-Sensing Characteristics of Exfoliated WSe2 Field-Effect Transistors, J. Nanosci. Nanotechnol. 17 (2017) 3151–3154.
[14] P K Panda, A Grigoriev, Y K Mishra, R Ahuja, Progress in supercapacitors: roles of two dimensional nanotubular materials, Nanoscale Adv. 2 (2020) 70–108.
[15] B Anasori, M R Lukatskaya, Y Gogotsi, 2D metal carbides and nitrides (MXenes) for energy storage, Nat. Rev. Mater. 2 (2017) 16098.
[16] C Anichini, W Czepa, D Pakulski, A Aliprandi, A Ciesielski, P Samorì, Chemical sensing with 2D materials, Chem. Soc. Rev. 47 (2018) 4860–4908.
[17] M Chhowalla, Z Liu, H Zhang, Two-dimensional transition metal dichalcogenide (TMD) nanosheets, Chem. Soc. Rev. 44 (2015) 2584–2586.
[18] W Choi, N Choudhary, G H Han, J Park, D Akinwande, Y H Lee, Recent development of two-dimensional transition metal dichalcogenides and their applications, Mater. Today 20 (2017) 116–130.
[19] Z Q Zheng, B Wang, J D Yao, G W Yang, Light-controlled C2H2 gas sensing based on Au–ZnO nanowires with plasmon-enhanced sensitivity at room temperature, J. Mater. Chem. C 3 (2015) 7067–7074.
[20] S Susarla, A Kutana, J A Hachtel, V Kochat, A Apte, R Vajtai, et al., 2D Materials: Quaternary 2D Transition Metal Dichalcogenides (TMDs) with Tunable Bandgap (Adv. Mater. 35/2017), Adv. Mater. (2017).
[21] L K Tan, B Liu, J H Teng, S Guo, H Y Low, K P Loh, Atomic layer deposition of a MoS2 film, Nanoscale 6 (2014) 10584–10588.
[22] M. Krbal, J. Prikryl, R. Zazpe, F. Dvorak, F. Bures, J.M. Macak, 2D MoSe2 Structures Prepared by Atomic Layer Deposition, physica status solidi (RRL) – Rapid Res. Lett., 12(2018) 1800023.
[23] N Rohaizad, C C Mayorga-Martinez, Z Sofer, M Pumera, 1T-Phase Transition Metal Dichalcogenides (MoS2, MoSe2, WS2, and WSe2) with Fast Heterogeneous Electron Transfer: Application on Second-Generation Enzyme-Based Biosensor, ACS Appl. Mater. Interfaces 9 (2017) 40697–40706.
[24] Y Han, D Huang, Y Ma, G He, J Hu, J Zhang, et al., Design of Hetero-Nanostructures on MoS2 Nanosheets To Boost NO2 Room-Temperature Sensing, ACS Appl. Mater. Interfaces 10 (2018) 22640–22649.
[25] K Y Ko, K Park, S Lee, Y Kim, W J Woo, D Kim, et al., Recovery Improvement for Large-Area Tungsten Diselenide Gas Sensors, ACS Appl. Mater. Interfaces 10 (2018) 23910–23917.
[26] K Y Ko, J-G Song, Y Kim, T Choi, S Shin, C W Lee, et al., Improvement of Gas-Sensing Performance of Large-Area Tungsten Disulfide Nanosheets by Surface Functionalization, ACS Nano 10 (2016) 9287–9296.

[27] T Xu, Y Liu, Y Pei, Y Chen, Z Jiang, Z Shi, et al., The ultra-high NO2 response of ultra-thin WS2 nanosheets synthesized by hydrothermal and calcination processes, Sens. Actuators, B 259 (2018) 789–796.
[28] J-K Huang, J Pu, C-L Hsu, M-H Chiu, Z-Y Juang, Y-H Chang, et al., Large-Area Synthesis of Highly Crystalline WSe2 Monolayers and Device Applications, ACS Nano 8 (2014) 923–930.
[29] B Liu, M Fathi, L Chen, A Abbas, Y Ma, C Zhou, Chemical Vapor Deposition Growth of Monolayer WSe2 with Tunable Device Characteristics and Growth Mechanism Study, ACS Nano 9 (2015) 6119–6127.
[30] H Long, A Harley-Trochimczyk, T He, T Pham, Z Tang, T Shi, et al., In Situ Localized Growth of Porous Tin Oxide Films on Low Power Microheater Platform for Low Temperature CO Detection, ACS Sensors 1 (2016) 339–343.
[31] H Li, G Lu, Y Wang, Z Yin, C Cong, Q He, et al., Mechanical Exfoliation and Characterization of Single- and Few-Layer Nanosheets of WSe2, TaS2, and TaSe2, Small 9 (2013) 1974–1981.
[32] D G Mead, J C Irwin, Long wavelength optic phonons in WSe2, Can. J. Phys. 55 (1977) 379–382.
[33] A Ambrosi, Z Sofer, M Pumera, 2H → 1T phase transition and hydrogen evolution activity of MoS2, MoSe2, WS2 and WSe2 strongly depends on the MX2 composition, Chem. Commun. 51 (2015) 8450–8453.
[34] N D Boscher, C J Carmalt, I P Parkin, Atmospheric pressure chemical vapor deposition of WSe2 thin films on glass—highly hydrophobic sticky surfaces, J. Mater. Chem. 16 (2006) 122–127.
[35] H Wang, D Kong, P Johanes, J J Cha, G Zheng, K Yan, et al., MoSe2 and WSe2 Nanofilms with Vertically Aligned Molecular Layers on Curved and Rough Surfaces, Nano Lett. 13 (2013) 3426–3433.
[36] W Yan, A Harley-Trochimczyk, H Long, L Chan, T Pham, M Hu, et al., Conductometric gas sensing behavior of WS2 aerogel, FlatChem 5 (2017) 1–8.
[37] S-Y Cho, S J Kim, Y Lee, J-S Kim, W-B Jung, H-W Yoo, et al., Highly Enhanced Gas Adsorption Properties in Vertically Aligned MoS2 Layers, ACS Nano 9 (2015) 9314–9321.
[38] W Yan, M A Worsley, T Pham, A Zettl, C Carraro, R Maboudian, Effects of ambient humidity and temperature on the NO2 sensing characteristics of WS2/graphene aerogel, Appl. Surf. Sci. 450 (2018) 372–379.
[39] R Guo, Y Han, C Su, X Chen, M Zeng, N Hu, et al., Ultrasensitive room temperature NO2 sensors based on liquid phase exfoliated WSe2 nanosheets, Sens. Actuators, B 300 (2019) 127013.
[40] W.S. Lee, J. Choi, Two-Dimensional Tungsten Diselenides Integrated on Paper Substrate for Highly Flexible and Sensitive Gas Sensor, 2019 20th International Conference on Solid-State Sensors, Actuators and Microsystems & Eurosensors XXXIII (TRANSDUCERS & EUROSENSORS XXXIII)2019, pp. 681-4.
[41] V N Mishra, R P Agarwal, Sensitivity, response and recovery time of SnO2 based thick-film sensor array for H2, CO, CH4 and LPG, Microelectron. J. 29 (1998) 861–874.
[42] N. Joshi, L.F. da Silva, H. Jadhav, J.-C. M'Peko, B.B. Millan Torres, K. Aguir, et al., One-step approach for preparing ozone gas sensors based on hierarchical NiCo2O4 structures, RSC Adv., 6(2016) 92655-62.
[43] T Wang, R Zhao, X Zhao, Y An, X Dai, C Xia, Tunable donor and acceptor impurity states in a WSe2 monolayer by adsorption of common gas molecules, RSC Adv. 6 (2016) 82793–82800.
[44] N Joshi, L F da Silva, H S Jadhav, F M Shimizu, P H Suman, J-C M'Peko, et al., Yolk-shelled ZnCo2O4 microspheres: Surface properties and gas sensing application, Sens. Actuators, B 257 (2018) 906–915.
[45] M. Enachi, O. Lupan, T. Braniste, A. Sarua, L. Chow, Y.K. Mishra, et al., Integration of individual TiO2 nanotube on the chip: Nanodevice for hydrogen sensing, physica status solidi (RRL) – Rapid Research Letters, 9(2015) 171-4.
[46] N Joshi, L F da Silva, F M Shimizu, V R Mastelaro, J-C M'Peko, L Lin, et al., UV-assisted chemiresistors made with gold-modified ZnO nanorods to detect ozone gas at room temperature, Microchim. Acta 186 (2019) 418.
[47] D J Late, Y-K Huang, B Liu, J Acharya, S N Shirodkar, J Luo, et al., Sensing Behavior of Atomically Thin-Layered MoS2 Transistors, ACS Nano 7 (2013) 4879–4891.
[48] H Long, L Chan, A Harley-Trochimczyk, L E Luna, Z Tang, T Shi, et al., 3D MoS2 Aerogel for Ultrasensitive NO2 Detection and Its Tunable Sensing Behavior, Adv. Mater. Interfaces 4 (2017) 1700217.
[49] R K Jha, P K Guha, Humidity Sensing Properties of Coexfoliated Heterogeneous WS_2WSe_2 Nanohybrids, IEEE Trans. Nanotechnol. 17 (2018) 582–589.
[50] V.A. Kuznetsov, A.Y. Ledneva, S.B. Artemkina, M.N. Kozlova, G.E. Yakovleva, A.S. Berdinsky, et al., Tungsten dichalcogenides as possible gas-sensing elements, 2017 40th International Convention on Information and Communication Technology, Electronics and Microelectronics (MIPRO)2017, pp. 48-52.